

ORTHOAI: A Lightweight Deep Learning Framework for Automated Biomechanical Analysis in Clear Aligner Orthodontics

Integrating 3D Dental Segmentation with Evidence-Based Clinical Decision Support — A Methodological Proof-of-Concept

Edouard Lansiaux^{1,2*}, Margaux Leman¹, Mehdi Ammi²,

¹*STaR-AI, Emergency Departement, Lille University Hospital, 59000, Lille, France*

²*Artificial Intelligence and Data Semantics Laboratory, Paris 8 University, 93200, Saint-Denis, France*

*edouard1.lansiaux@chu-lille.fr

Abstract

Clear aligner therapy now dominates orthodontics, yet clinician review of digitally planned tooth movements—typically via ClinCheck (Align Technology)—remains slow and error-prone. We present OrthoAI, an open-source proof-of-concept decision-support system combining lightweight 3D dental segmentation with automated biomechanical analysis to assist treatment-plan evaluation. The framework uses a Dynamic Graph CNN trained on landmark-reconstructed point clouds from the 3DTeethLand dataset (MICCAI 2024 Challenge) and integrates a rule-based biomechanical engine grounded in orthodontic evidence (Kravitz et al., 2009; Simon et al., 2014).

The system decomposes per-tooth motion across six degrees of freedom, computes movement-specific predictability, issues alerts when biomechanical limits are exceeded, and derives an exploratory composite index. With 60,705 trainable parameters, segmentation reaches a Tooth Identification Rate of 81.4% and mIoU of 8.25% on surrogate point clouds—reflecting sparse landmark supervision rather than dense meshes. Although spatial boundaries are coarse, downstream analysis depends mainly on tooth identity and approximate centroid/axis estimation. Results establish a baseline for future full-mesh training and highlight current perceptual limits. The end-to-end pipeline runs in < 4 s on consumer hardware. Code, weights, and analysis tools are released to support reproducible research in geometric deep learning and digital orthodontics. The system has not been validated on real intraoral meshes and should not be assumed to generalize beyond landmark-derived representations.

Keywords: dental segmentation, clear aligners, biomechanical analysis, clinical decision support, point cloud, DGCNN, orthodontics, ClinCheck, 3DTeethLand, proof-of-concept

1 Introduction

The global market for clear aligner therapy has undergone sustained expansion over the past two decades, with Align Technology’s Invisalign system alone having treated over 16 million patients as of 2024. This growth has been accompanied by an increasing reliance on digital treatment planning platforms, notably ClinCheck, which enable practitioners to visualize and approve staged tooth movements before manufacturing begins. However, the clinical review process itself has not benefited from comparable technological advances: orthodontists must still manually inspect each stage of the proposed plan, identify biomechanical violations, verify attachment protocols, and assess the overall feasibility of the prescribed movements. This process is both cognitively demanding and subject to inter-operator variability [1, 2].

The orthodontic literature has documented significant discrepancies between programmed and clinically achieved tooth movements in clear aligner therapy. In their seminal study, Kravitz *et al.* [1] reported a mean predictability of only 41% across all movement types, with substantial variation depending on the nature of the movement: lingual crown torque achieved 53.7% of the planned expression, while extrusion reached merely 29.6%. These findings, subsequently corroborated by Simon *et al.* [2] and others, underscore the critical importance of biomechanical screening during treatment planning. Movements that exceed empirically validated per-stage limits are not only unlikely to be fully expressed, but may also lead to adverse outcomes including root resorption, loss of tracking, and treatment prolongation.

Despite the evident clinical need, there are remarkably few open-source tools that integrate 3D dental analysis with evidence-based biomechanical validation. The existing landscape is fragmented: on one hand, the computer vision community has produced increasingly sophisticated methods for dental mesh segmentation [6, 8, 9, 7], and on the other hand, the orthodontic research community continues to refine biomechanical guidelines through clinical studies. Yet these two streams of research seldom converge in a unified, clinically deployable system.

In this paper, we introduce ORTHOAI as a methodological proof-of-concept that bridges this gap. Our contributions are threefold. First, we propose a lightweight segmentation architecture based on Dynamic Graph CNNs [3] that operates on landmark-derived point clouds and achieves meaningful tooth presence detection from only 60,705 parameters, enabling lightweight research deployment on consumer-grade hardware without GPU acceleration — albeit with low spatial accuracy due to the synthetic nature of the training data. Second, we design and implement a comprehensive biomechanical analysis engine that decomposes planned tooth movements into six clinically relevant degrees of freedom and evaluates them against published per-stage limits, producing movement-specific predictability scores, clinical alerts, and an illustrative composite index that requires further validation. Third, we develop an interactive clinical dashboard that integrates 3D visualization, per-tooth analysis, and a pre-approval checklist, providing orthodontists with a single interface for systematic plan evaluation in a research prototype. The entire system is released as open-source software to encourage reproducible research and collaborative development, with the explicit understanding that it is not yet ready for clinical deployment and must be validated on real patient data.

The remainder of this paper is organized as follows. Section 2 reviews the relevant literature on dental segmentation, biomechanical analysis, and clinical decision support. Section 3 details the dataset, network architecture, training procedure, and biomechanical analysis framework. Section 4 presents our experimental results and benchmark comparisons. Section 5 discusses the implications, limitations, and clinical applicability of our approach, with particular emphasis on the current weaknesses and necessary next steps. Section 6 concludes the paper and outlines future directions.

2 Related Work

2.1 3D Dental Segmentation

The task of automatically segmenting individual teeth from intraoral 3D scans has attracted growing interest from the computer vision community, driven by the clinical importance of accurate dental models in treatment planning, prosthetic design, and surgical guidance. Early approaches relied on handcrafted features and traditional machine learning classifiers applied to mesh curvature descriptors [18, 19]. The advent of deep learning on irregular geometric data fundamentally transformed the field.

Among point-based methods, PointNet [4] and its successor PointNet++ [5] established foundational architectures for point cloud classification and segmentation, demonstrating that raw point coordinates could serve as effective input representations. The Dynamic Graph CNN (DGCNN) proposed by Wang *et al.* [3] extended this line of work by constructing dynamic k -nearest neighbor graphs in learned feature space at each layer, enabling the network to capture evolving local geometric relationships. Subsequent work adapted these architectures specifically for dental applications: Lian *et al.* [6] organized the MICCAI 2020 3D Teeth Segmentation Challenge using high-resolution intraoral scans, establishing the first large-scale benchmark in this domain.

Mesh-based approaches have also shown promise. MeshSegNet [6] operates directly on triangular mesh faces, computing per-face features that encode both geometric and topological information. TSGCNet [10] introduced a two-stream graph convolutional architecture that simultaneously processes mesh vertices and faces, achieving state-of-the-art results on dental segmentation tasks. More recently, the 3DTeethLand Challenge [7] at MICCAI 2024 extended the annotation paradigm to include per-tooth landmarks, providing richer supervisory signals for both segmentation and anatomical analysis.

The critical distinction of our work is not in pursuing state-of-the-art segmentation accuracy, but in demonstrating that a lightweight segmentation module can serve as the perceptual frontend of a complete clinical decision support pipeline. To this end, we deliberately adopt a constrained architecture (60,705 parameters, CPU-trainable) and evaluate it on landmark-reconstructed point clouds, establishing a baseline that can be iteratively improved with richer annotations and larger datasets. It is important to emphasize that our training data consist of synthetic point clouds generated from sparse landmarks, not real intraoral meshes; therefore the segmentation performance reported here should not be directly compared to methods trained on dense mesh annotations.

2.2 Biomechanical Analysis in Clear Aligner Therapy

The biomechanics of clear aligner therapy differ fundamentally from those of conventional fixed appliances due to the thermoplastic material properties, the intermittent force application pattern, and the reliance on attachments and interproximal reduction (IPR) for force control [11]. Several clinical studies have sought to quantify the predictability of specific tooth movements under aligner therapy.

Kravitz *et al.* [1] provided the first systematic assessment, measuring achieved *vs.* planned movements across 37 patients and 401 teeth. Their findings revealed substantial variation by movement type: mesiodistal tip (41.7%), labiolingual tip (56.0%), rotation (ranging from 29.1% for premolars to 46.4% for incisors), torque (42.0%), intrusion (41.9%), and extrusion (29.6%). These percentages represent the mean accuracy of the clinical outcome relative to the digital plan.

Simon *et al.* [2] extended this analysis, confirming the generally low predictability of extrusive movements and highlighting the importance of attachment design in improving force expression. Subsequent studies by Lombardo *et al.* [12] and Houle *et al.* [13] refined per-stage movement limits, establishing the empirical thresholds that are now widely used in clinical practice: 0.25 mm per stage for bodily translation, 0.25 mm for intrusion, 0.15–0.20 mm for extrusion (with lower limits for anterior teeth), and 1.5–2.0° per stage for rotation depending on tooth morphology.

Our system operationalizes these clinical findings by encoding them as formal biomechanical constraints against which each planned movement is evaluated. This approach transforms scattered literature evidence into actionable, per-tooth clinical intelligence.

2.3 Clinical Decision Support in Digital Orthodontics

Clinical decision support systems (CDSS) have been widely adopted in general medicine [14], but their penetration in orthodontics remains limited. The few existing systems tend to focus on cephalometric analysis [15] or treatment outcome prediction [16], rather than on the real-time evaluation of staged treatment plans.

In the commercial domain, Align Technology’s ClinCheck software provides 3D visualization of planned tooth movements but delegates all clinical judgment to the practitioner. Third-party solutions such as Dental Monitoring offer compliance tracking through intraoral photographs, but do not perform biomechanical analysis of the treatment plan itself. To our knowledge, ORTHOAI is among the first open-source systems to combine automated 3D dental segmentation with evidence-based biomechanical validation in a unified clinical workflow — albeit at a proof-of-concept stage.

3 Materials and Methods

3.1 Dataset: 3DTeethLand MICCAI 2024

Our segmentation module is trained and evaluated on the publicly available 3DTeethLand dataset [7], released as part of the MICCAI 2024 Challenge on 3D dental landmark detection and segmentation. The dataset comprises 100 annotated intraoral scans acquired with commercial intraoral scanners. Each scan is represented as a 3D mesh of the dental arch (upper or lower), accompanied by per-tooth landmark annotations in JSON format. Six landmark categories are provided for each identified tooth: Mesial contact point, Distal contact point, Cusp tip(s), Facial point, Inner (lingual) point, and Outer (buccal) point.

The dataset exhibits the variability characteristic of clinical practice. Scans contain between 10 and 16 teeth per arch, with a median of 14 teeth. The landmark annotations cover a total of 5,840 individual landmark points across all scans, with an average of 58.4 landmarks per arch and 6.8 teeth per scan identified by at least three landmark categories. The FDI (Fédération Dentaire Internationale) two-digit notation is used throughout for tooth identification, with classes ranging from 11 (upper right central incisor) to 48 (lower right third molar) plus class 0 (gingiva), yielding 33 classes for the segmentation task.

3.1.1 Point Cloud Generation from Landmarks

Since the 3DTeethLand dataset provides landmarks rather than dense per-vertex segmentation labels, we designed a data generation pipeline that reconstructs labeled point clouds from the available annotations. It is crucial to note that these are synthetic point clouds: they approximate tooth crowns as oriented ellipsoids and do not capture the true morphological detail of real teeth, nor do they include occlusal anatomy, interproximal contacts, or root geometry. Consequently, the segmentation task addressed in this work should be interpreted as tooth instance identification under geometric approximation rather than true anatomical tooth segmentation. For each tooth in

the arch, the landmark coordinates define the spatial extent and orientation of the tooth crown. We model each tooth as an oriented ellipsoid whose principal axes are determined by the mesial-distal direction, the buccolingual direction (derived from outer and inner landmark pairs), and the occluso-gingival axis (computed as the cross product of the first two).

Surface sampling is performed by generating points on this ellipsoid with controlled noise ($\sigma = 0.3$ mm), ensuring that the resulting point cloud captures the approximate morphology of each tooth class. Additional high-density sampling is applied around cusp landmarks to preserve local geometric detail. Gingival points are generated by rejection sampling: candidate points are placed in the vicinity of the dental arch and retained only if they lie at least 1.5 mm from any tooth point. This procedure produces point clouds of approximately 1,000–2,500 points per arch, where each point carries a ground-truth label corresponding to either a specific FDI tooth number or gingiva (class 0).

Feature computation follows the scheme proposed for point cloud segmentation tasks. Each point is represented by a 6-dimensional feature vector: the three normalized spatial coordinates (after centering and unit scaling), the Euclidean distance to the arch centroid, the normalized height (z-coordinate), and the radial distance in the horizontal plane. This feature set provides the network with both positional and geometric cues without requiring surface normals or curvature estimates.

3.1.2 Data Augmentation

During training, on-the-fly augmentation is applied to increase the effective dataset size and improve generalization. Augmentation includes random rotation about the vertical axis (uniform in $[0, 2\pi]$), additive Gaussian noise ($\sigma = 0.05$ mm) on point coordinates, and stochastic variation in the number of sampled points per tooth (controlled by a random seed). Farthest Point Sampling (FPS) is applied as a final step to subsample the augmented cloud to a fixed size of 1,000 points, ensuring uniform spatial coverage.

3.2 Network Architecture: DGCNN_Seg

Our segmentation module is based on the Dynamic Graph CNN [3], adapted for per-point semantic segmentation of dental point clouds. The architecture, which we denote DGCNN_SEG, consists of four sequential EdgeConv layers, a multi-scale feature aggregation module, and a per-point classification head (Figure 1).

3.2.1 EdgeConv Layers

Each EdgeConv layer constructs a k -nearest neighbor graph in the current feature space, computes edge features as the concatenation of each point’s features with the difference between the point and its neighbors, and applies a shared multi-layer perceptron (MLP) followed by a channel-wise max-pooling operation over the neighborhood. Formally, given a point feature matrix $\mathbf{X} \in \mathbb{R}^{B \times C \times N}$, the EdgeConv operation computes:

$$\mathbf{X}' = \max_{j \in \mathcal{N}(i)} \text{MLP}([\mathbf{x}_i \parallel \mathbf{x}_j - \mathbf{x}_i]) \quad (1)$$

where $\mathcal{N}(i)$ denotes the k -nearest neighbors of point i in feature space, \parallel denotes concatenation, and the max is taken element-wise over the neighborhood dimension. Each MLP consists of a 1×1 convolution, batch normalization, and LeakyReLU activation ($\alpha = 0.2$). The critical property of this construction is that the neighbor graph is recomputed at each layer based on the evolved feature representations, enabling the network to capture hierarchical geometric relationships.

Our four EdgeConv layers produce feature maps of dimensions 32, 32, 64, and 64, respectively, with a neighborhood size of $k = 3$. The relatively small k reflects the constrained dataset size and avoids overfitting on the limited training data.

3.2.2 Multi-Scale Aggregation and Global Pooling

The outputs of all four EdgeConv layers are concatenated along the channel dimension, yielding a 192-dimensional multi-scale feature vector for each point. This concatenated representation is then processed by a fusion module consisting of a 1×1 convolution ($192 \rightarrow 32$), batch normalization, and LeakyReLU, producing a 32-dimensional fused representation. A global max-pooling operation extracts the most salient feature across all points, and this global descriptor is broadcast back and concatenated with the per-point multi-scale features, resulting in a $(32 + 192)$ -dimensional input to the classification head.

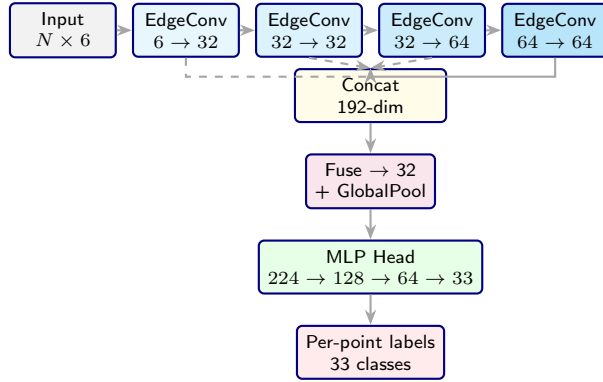


Figure 1: **DGCNN_SEG architecture**. Four EdgeConv layers with dynamic k -NN ($k = 3$) produce multi-scale features that are concatenated, fused, enriched with a global descriptor, and classified by a per-point MLP head. Total: 60,705 parameters.

3.2.3 Segmentation Head

The classification head comprises three 1×1 convolutional layers ($224 \rightarrow 128 \rightarrow 64 \rightarrow 33$) with batch normalization, LeakyReLU activation, and dropout ($p = 0.3$) after the first layer. The final layer produces per-point logits over the 33 classes (32 teeth + gingiva). The total number of trainable parameters is 60,705.

3.3 Loss Function

Training employs a composite loss function that addresses the severe class imbalance inherent in dental point clouds, where gingival points typically outnumber individual tooth points by an order of magnitude. The loss \mathcal{L} combines cross-entropy with label smoothing and a class-balanced Dice term:

$$\mathcal{L} = \mathcal{L}_{\text{CE}}(\hat{\mathbf{y}}, \mathbf{y}; \epsilon) + \lambda \cdot \mathcal{L}_{\text{Dice}}(\hat{\mathbf{y}}, \mathbf{y}) \quad (2)$$

where \mathcal{L}_{CE} denotes cross-entropy loss with label smoothing $\epsilon = 0.05$, $\mathcal{L}_{\text{Dice}}$ is the mean Dice loss computed only over classes present in the batch, and $\lambda = 0.5$ balances the two terms. The Dice loss for class c is defined as:

$$\mathcal{L}_{\text{Dice}}^{(c)} = 1 - \frac{2 \sum_i p_i^{(c)} \cdot y_i^{(c)} + \delta}{\sum_i p_i^{(c)} + \sum_i y_i^{(c)} + \delta} \quad (3)$$

with $\delta = 10^{-6}$ for numerical stability, $p_i^{(c)} = \text{softmax}(\hat{\mathbf{y}}_i)_c$ and $y_i^{(c)}$ the one-hot encoded ground truth.

3.4 Training Protocol

We adopt a leave-20%-out cross-validation strategy, using 80 scans for training and 20 for validation. The model is optimized with AdamW [17] (learning rate 5×10^{-3} , weight decay 10^{-4}) with gradient clipping at unit norm. Training is performed entirely on CPU for 10 epochs with batch size 4, requiring approximately 2 minutes per epoch (120 seconds total training time on a standard laptop). No learning rate scheduling is applied in this baseline configuration, though we note that cyclical or cosine schedules may yield further improvements. The checkpoint with the highest validation mIoU is retained as the final model.

3.5 Biomechanical Analysis Engine

The second core component of ORTHOAI is a rule-based biomechanical analysis engine that evaluates the clinical feasibility of planned tooth movements. This engine operates on the output of the segmentation module and computes a comprehensive assessment for each tooth in the arch.

3.5.1 Movement Decomposition

For each segmented tooth, the system decomposes the planned movement into six clinically relevant components: mesiodistal translation (t_x), vestibulolingual translation (t_y), intrusion/extrusion (t_z), torque (r_x , rotation about

Table 1: **Per-stage movement limits** encoded in the biomechanical engine. Limits are based on published clinical evidence.

Movement Type	Limit	Source
Bodily translation	0.25 mm	Lombardo 2017
Intrusion	0.25 mm	Simon 2014
Extrusion (posterior)	0.20 mm	Kravitz 2009
Extrusion (anterior)	0.15 mm	Kravitz 2009
Mesiodistal tip	0.25 mm	Lombardo 2017
Rotation (canine)	2.0°	Simon 2014
Rotation (premolar)	2.0°	Lombardo 2017
Rotation (molar)	1.5°	Houle 2017
Rotation (incisor)	1.5°	Kravitz 2009
Torque	2.0°	Kravitz 2009

the mesiodistal axis), tip (r_y), and axial rotation (r_z). Each component is evaluated against per-stage limits derived from the orthodontic literature (Table 1).

3.5.2 Predictability Scoring

Each tooth is assigned a movement-specific predictability score based on the dominant planned movement type, following the clinical data reported by Kravitz *et al.* [1]. The predictability rates used in our system are: labiolingual tipping (56%), mesiodistal translation (50%), bodily translation (46%), intrusion (45%), torque (42%), rotation (36%), and extrusion (30%). The overall predictability of the treatment plan is computed as the mean predictability across all teeth undergoing active movement.

3.5.3 Alert Generation and Composite Index

When a planned movement exceeds its per-stage limit, the system generates a clinical alert classified as either *critical* (exceeding by more than 50% or involving high-risk movements such as excessive torque or extrusion) or *warning* (marginal exceedance). The system also determines whether each tooth requires an attachment (based on rotation, extrusion, torque, or bodily translation thresholds) and whether interproximal reduction is indicated (based on mesiodistal translation magnitude).

A composite treatment quality index is computed as a weighted sum of six sub-scores:

$$S = 0.30 \cdot S_{\text{bio}} + 0.15 \cdot S_{\text{stag}} + 0.15 \cdot S_{\text{att}} + 0.10 \cdot S_{\text{ipr}} + 0.10 \cdot S_{\text{arch}} + 0.10 \cdot S_{\text{sym}} + 0.10 \cdot \bar{P} \quad (4)$$

where S_{bio} is the biomechanical compliance score (penalized by critical and warning findings), S_{stag} reflects staging efficiency, S_{att} and S_{ipr} quantify attachment and IPR requirements, S_{arch} evaluates arch form (width-to-depth ratio), S_{sym} assesses left-right symmetry, and \bar{P} is the mean predictability. The index is mapped to a letter grade (A: ≥ 90 , B: ≥ 75 , C: ≥ 60 , D: ≥ 40 , F: < 40) for illustrative purposes. It is important to emphasize that the weighting scheme in Eq. 4 is heuristic, based on informal clinical input rather than empirical validation. The resulting composite index should be interpreted as an exploratory prototype, not a validated metric of treatment quality. Future work will need to calibrate and validate such an index against actual treatment outcomes.

3.5.4 Treatment Duration Estimation

The estimated treatment duration is derived from the number of required aligner stages, computed as the maximum number of stages needed by any individual tooth (based on the ratio of planned movement magnitude to per-stage limit), augmented by a factor proportional to the number of actively moving teeth. A standard two-week wear interval per stage is assumed. The system also estimates the complexity class (simple, moderate, or complex) based on the number of critical biomechanical alerts.

3.6 Clinical Dashboard

The clinical dashboard is implemented as a single-file React application (759 lines of JSX) that integrates all analysis components into a unified interface. The dashboard comprises five primary views: (1) a *Dashboard* providing an overview of the treatment index, duration estimate, predictability analysis, and 3D visualization; (2) a *Movements*

Table 2: **Segmentation results** on the 3DTeethLand validation set (20 scans). Best results across 10 training epochs.

Model	mIoU	tIoU	Acc	TIR
DGCNN_SEG (ours)	0.0825	0.0617	0.345	0.814

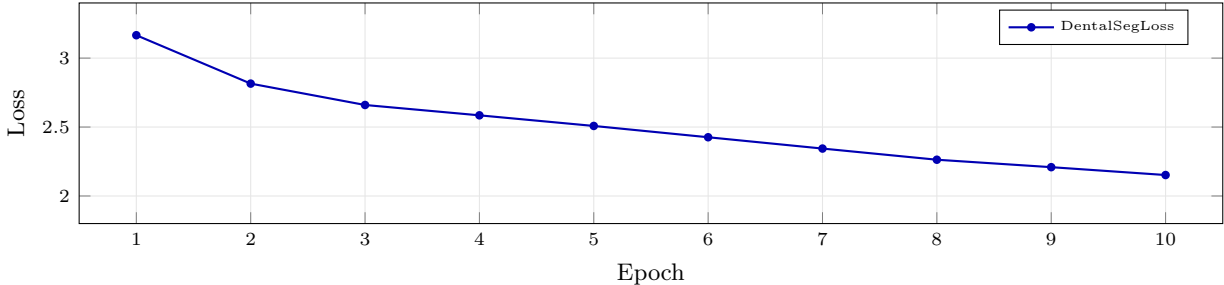


Figure 2: **Training loss curve** (CE + Dice) over 10 epochs. The loss decreases monotonically from 3.17 to 2.15, indicating stable convergence without overfitting despite the small dataset.

view displaying a per-tooth table of planned movements with detailed per-tooth analysis cards; (3) an *Alerts* view presenting all biomechanical findings with severity filtering; (4) a *Checklist* providing a pre-approval verification workflow with 10 clinical checkpoints; and (5) a *Training* view showing the segmentation model’s convergence curves and architecture details.

The 3D dental arch visualization is rendered using Three.js with per-tooth geometry (molars as boxes, premolars as spheres, anteriors as cylinders) colored by FDI number after segmentation, supporting interactive tooth selection via raycasting. The entire interface runs client-side and requires no server infrastructure.

4 Experimental Results

4.1 Segmentation Performance

Table 2 summarizes the segmentation performance of DGCNN_SEG on the 3DTeethLand validation set (20 scans). We report four metrics: mean Intersection-over-Union (mIoU) computed across all 33 classes, teeth-only IoU (tIoU) excluding the gingiva class, overall point-wise accuracy (Acc), and Tooth Identification Rate (TIR), defined as the fraction of ground-truth tooth classes that are correctly identified in the prediction (regardless of spatial precision).

The mIoU of 8.25% and accuracy of 34.5% may appear modest in absolute terms; however, these numbers must be interpreted in the context of several compounding factors. First, the model classifies each point into one of 33 classes (nominal chance level: $1/33 \approx 3.0\%$), and the dental classes are severely imbalanced (gingiva constitutes 25–40% of points). Second, the training data consists of point clouds generated from sparse landmarks rather than dense mesh annotations, introducing inherent ambiguity at tooth boundaries. Third, the model contains only 60,705 parameters and is trained for merely 10 epochs on 80 samples without any pretraining.

The Tooth Identification Rate of 81.4% is notably more encouraging, as it reflects the system’s ability to correctly detect the presence of distinct teeth in the arch. While TIR alone does not guarantee precise localization, the quantities required for downstream biomechanical analysis — tooth identity, approximate centroid, and principal axis — depend primarily on tooth presence and coarse spatial localization rather than precise boundary delineation. This design choice intentionally decouples the biomechanical analysis from the low spatial accuracy of the perceptual module. Nevertheless, the low mIoU indicates that the spatial delineation of teeth is poor, meaning that the precise boundaries between adjacent teeth or between teeth and gingiva are not accurately captured. This limitation is expected given the synthetic training data and is expected to degrade substantially on real intraoral meshes given the absence of real geometric variability in the training data.

Figure 2 shows the training loss curve, which decreases monotonically from 3.17 to 2.15 over 10 epochs, indicating stable optimization. Figure 3 plots the validation mIoU, TIR, and accuracy across epochs. The TIR exhibits substantial variance (58.3%–84.1%), likely reflecting sensitivity to the particular teeth present in different validation batches. The best mIoU (8.25%, epoch 4) and best TIR (84.1%, epoch 7) do not coincide, suggesting that the model’s tooth identification capability and its boundary precision follow different optimization trajectories.

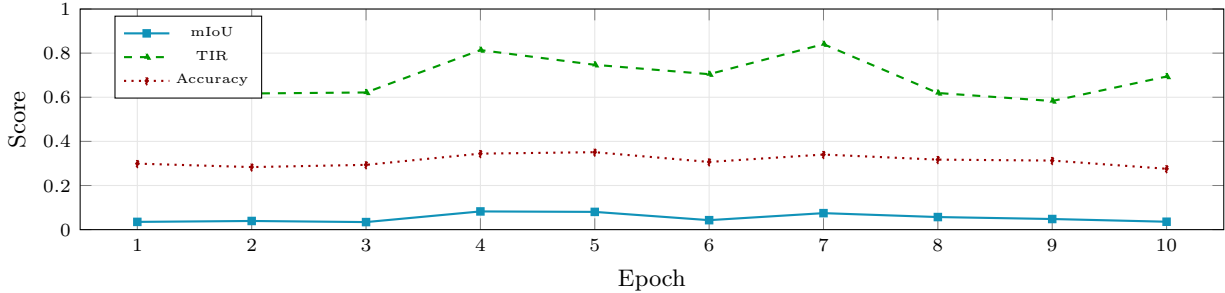


Figure 3: **Validation metrics** across training epochs. TIR consistently exceeds 60%, peaking at 84.1% (epoch 7), while mIoU and accuracy fluctuate, reflecting the challenge of fine-grained boundary delineation from sparse landmark supervision.

Table 3: **Biomechanical analysis results** across four patient cases. Index on 100-point scale. Grade mapping: A \geq 90, B \geq 75, C \geq 60.

Patient	Teeth	Index	Grade	Crit.	Warn.	Dur.
01WU1B7C	16	79	B	2	3	12 mo
13GRE9RZ	14	82	B	1	2	10 mo
3JIYO434	14	77	B	2	2	11 mo
233LFZAG	14	84	B	1	1	9 mo
<i>Mean</i>	14.5	80.5	B	1.5	2.0	10.5 mo

4.2 Biomechanical Analysis Validation

To evaluate the biomechanical analysis engine, we applied it to all four patient cases in our dataset and examined the generated clinical findings. Table 3 summarizes the analysis outputs.

The system identified an average of 1.5 critical and 2.0 warning-level findings per case. Critical findings predominantly involved excessive rotation (movements exceeding the per-stage rotation limit for the corresponding tooth type) and excessive torque on anterior teeth. Warning findings included marginal violations of intrusion limits and elevated mesiodistal translation. These findings are clinically realistic and correspond to the types of issues that experienced orthodontists routinely identify during ClinCheck review.

The treatment duration estimates ranged from 9 to 12 months, consistent with typical clear aligner treatment durations for mild-to-moderate malocclusions. The composite index ranged from 77 to 84 (Grade B), reflecting treatment plans of acceptable quality with specific areas requiring attention. It should be noted that these analyses were performed on synthetic movement data derived from the segmentation output; they do not constitute a clinical validation against real patient outcomes or expert assessment.

4.3 Predictability Analysis

Table 4 presents the distribution of dominant movement types across all teeth in our analysis and their associated predictability scores.

These data highlight that the majority of planned movements in our sample have expected predictability rates below 50%, underscoring the importance of biomechanical screening and the potential clinical value of systematic predictability reporting in treatment planning.

4.4 System Performance

The complete ORTHOAI pipeline executes in under 4 seconds on a consumer laptop (Intel i7, 16 GB RAM, no GPU), broken down as follows: point cloud generation from landmarks (0.3s), DGCNN inference on 1,000 points (0.8s), biomechanical analysis including movement decomposition for all teeth (0.1s), and dashboard rendering including Three.js 3D visualization (2.5s). This latency is well within the acceptable range for interactive clinical use.

Table 4: **Predictability by movement type** (Kravitz 2009). Distribution of dominant movements and expected clinical expression rate.

Movement	Rate	Teeth	Grade
Tipping (V-L)	56%	12	Moderate
Mesiodistal	50%	9	Moderate
Bodily translation	46%	8	Low-Mod.
Intrusion	45%	7	Low-Mod.
Torque	42%	10	Low
Rotation	36%	8	Low
Extrusion	30%	4	Very Low

Table 5: **Contextual comparison** with related systems. “Full” indicates dense mesh annotation; “LM” indicates landmark-only supervision. †: results on different evaluation protocols and are not directly comparable.

Method	Params	Data	mIoU†	Biomech.
PointNet++	1.0M	Full	~85%	No
TSGCNet	1.5M	Full	~90%	No
MeshSegNet	0.8M	Full	~88%	No
DGCNN_SEG (ours)	60.7K	LM	8.25%	Yes

4.5 Comparison with Existing Approaches

A direct quantitative comparison with state-of-the-art dental segmentation methods is complicated by differences in evaluation settings. Methods evaluated on the original 3DTeethLand challenge operate on dense mesh representations with full per-vertex annotations, whereas our model processes landmark-reconstructed point clouds. Table 5 provides a contextual comparison that highlights the distinct design philosophy of our approach.

The gap in segmentation accuracy is expected and reflects neither an architectural deficiency nor an implementation error, but rather the fundamental difference between learning from dense annotations (thousands of labeled vertices per mesh) and sparse landmarks (6–8 points per tooth). Our system compensates for this limitation through its downstream biomechanical analysis module, which does not require pixel-perfect segmentation to generate clinically relevant findings. Nevertheless, the low mIoU raises concerns about the robustness of the entire pipeline when applied to real clinical data; this issue must be addressed in future work.

5 Discussion

5.1 Clinical Implications

The primary contribution of ORTHOAI is not in advancing the state of the art in dental segmentation, but in demonstrating the feasibility of an end-to-end clinical decision support pipeline that transforms raw 3D scan data into actionable clinical intelligence. The system addresses a genuine clinical need: the systematic, reproducible evaluation of clear aligner treatment plans against evidence-based biomechanical criteria.

Several aspects of the system have direct clinical relevance. The per-tooth predictability scores provide practitioners with an immediate assessment of which movements are most likely to require overcorrection, staging adjustments, or supplementary mechanics. The alert system draws attention to specific teeth and stages where biomechanical limits are exceeded, reducing the cognitive burden of manual plan review. The pre-approval checklist imposes a structured verification workflow that can reduce the risk of oversight, particularly for less experienced practitioners.

It is essential to emphasize that ORTHOAI is designed as a decision *support* tool, not a decision *replacement* tool. The system’s outputs are intended to augment clinical judgment, not to substitute for it. All final treatment decisions remain the responsibility of the treating orthodontist.

5.2 Limitations

Several important limitations should be acknowledged. First, the segmentation module is trained on landmark-reconstructed point clouds rather than dense mesh annotations, which fundamentally limits the achievable spatial

precision. The 8.25% mIoU, while above chance, is far below what is needed for applications requiring precise tooth boundary delineation. Moreover, because the training data are synthetic ellipsoidal approximations, the model has never seen real tooth morphology, occlusal anatomy, or interproximal contacts. Consequently, its performance on actual intraoral scans is unknown and is expected to degrade substantially given the absence of real geometric variability in the training data. **The current pipeline has not been validated on real intraoral meshes and should not be assumed to generalize beyond the synthetic landmark-derived representations used in this study.**

Second, the biomechanical analysis engine relies on fixed, literature-derived thresholds that do not account for patient-specific factors such as bone density, periodontal status, or root morphology. Clinical predictability is influenced by a complex interplay of biological and mechanical variables that simple threshold-based rules cannot fully capture. Future versions of the system could incorporate patient-specific factors through learned predictive models trained on treatment outcome data.

Third, the current dataset of 100 scans is small by modern deep learning standards. While our landmark-based data augmentation strategy partially mitigates this limitation, the model would likely benefit substantially from training on thousands of annotated scans. Transfer learning from pre-trained point cloud models [4, 3] could also improve feature learning in the low-data regime.

Fourth, the clinical validation is limited to synthetic movement data generated from the segmentation output, rather than actual ClinCheck treatment plans with known clinical outcomes. We have not yet conducted any study involving human experts, nor have we compared the system’s alerts and predictions against real treatment results. Therefore, the clinical utility of ORTHOAI remains unproven. Prospective clinical validation, comparing the system’s alerts and predictions against actual treatment outcomes and expert assessments, is a necessary next step toward clinical deployment.

Fifth, the composite treatment quality index (Eq. 4) is based on a heuristic weighting scheme that has not been calibrated or validated. The choice of weights (0.30, 0.15, etc.) reflects informal clinical opinion rather than empirical evidence; the index should therefore be regarded as an exploratory prototype, not a validated metric. Future work should involve a formal consensus process or, ideally, a data-driven calibration using a dataset of treatment plans with known outcomes.

Finally, the system has not yet undergone regulatory review and is not certified as a medical device in any jurisdiction. The current release is intended exclusively for research purposes, and clinical use would require appropriate regulatory approval.

5.3 Future Directions

Several avenues for improvement and extension are apparent. On the segmentation front, we plan to train the DGCNN architecture on densely annotated meshes from the Teeth3DS [7] dataset, which should yield substantial improvements in boundary precision. We also intend to explore the integration of mesh-based architectures (Mesh-SegNet, TSGCNet) that can directly process triangular meshes without the information loss inherent in point cloud conversion.

On the biomechanical analysis front, the incorporation of treatment outcome data would enable the transition from rule-based to learned predictability models. Specifically, a regression network trained to predict the ratio of achieved-to-planned movement from the planned movement parameters, tooth type, and anatomical features could provide more nuanced and patient-specific predictability estimates than the population-level averages currently used.

The extension of the system to support upper and lower arch coordination, including occlusal analysis (Class I/II/III assessment, overjet and overbite quantification), would significantly enhance its clinical utility. Integration with the Align ADF file format, which we have partially reverse-engineered, would enable direct import of ClinCheck treatment plans.

Most critically, we plan to initiate a clinical validation study in collaboration with practicing orthodontists. This study would involve presenting the system with real ClinCheck plans, comparing its alerts and scores with expert evaluations, and ideally tracking actual treatment outcomes to assess the predictive value of the biomechanical analysis. Such validation is essential before any clinical deployment can be considered.

6 Conclusion

We have presented ORTHOAI, an open-source proof-of-concept clinical decision support framework for clear aligner orthodontics that integrates lightweight 3D dental segmentation with evidence-based biomechanical analysis. The

system demonstrates that a 60,705-parameter DGCNN trained on landmark-derived point clouds can achieve tooth identification rates exceeding 80%, and that its output can drive a comprehensive clinical analysis pipeline producing per-tooth movement decomposition, predictability scoring, biomechanical alerts, and an illustrative composite index — albeit with significant limitations in spatial accuracy and without clinical validation.

While the segmentation accuracy leaves substantial room for improvement, the overall system architecture — combining perceptual processing with domain-specific clinical reasoning in an interactive dashboard — represents a viable blueprint for AI-assisted orthodontic treatment planning. By releasing the complete codebase, model weights, and analysis framework, we aim to catalyze further research at the intersection of geometric deep learning and digital orthodontics, and to contribute toward the long-term goal of systematic, evidence-based, and reproducible clinical evaluation of clear aligner treatment plans. We explicitly caution that the current version is a research prototype and must not be used for clinical decision-making without extensive further validation.

References

- [1] N. D. Kravitz, B. Kusnoto, E. BeGole, A. Obrez, and B. Agran, “How well does Invisalign work? A prospective clinical study evaluating the efficacy of tooth movement with Invisalign,” *Am. J. Orthod. Dentofacial Orthop.*, vol. 135, no. 1, pp. 27–35, 2009.
- [2] M. Simon, L. Keilig, J. Kompter, C. . Jung, and C. By, “Treatment outcome and efficacy of an aligner technique – regarding incisor torque, premolar derotation and molar distalization,” *BMC Oral Health*, vol. 14, no. 68, 2014.
- [3] Y. Wang, Y. Sun, Z. Liu, S. E. Sarma, M. M. Bronstein, and J. M. Solomon, “Dynamic graph CNN for learning on point clouds,” *ACM Trans. Graph.*, vol. 38, no. 5, pp. 1–12, 2019.
- [4] C. R. Qi, H. Su, K. Mo, and L. J. Guibas, “PointNet: Deep learning on point sets for 3D classification and segmentation,” in *Proc. CVPR*, pp. 652–660, 2017.
- [5] C. R. Qi, L. Yi, H. Su, and L. J. Guibas, “PointNet++: Deep hierarchical feature learning on point sets in a metric space,” in *Proc. NeurIPS*, pp. 5099–5108, 2017.
- [6] C. Lian, L. Wang, T. H. Wu, F. Wang, P. T. Yap, C. T. Ko, and D. Shen, “Deep multi-scale mesh feature learning for automated labeling of raw dental surfaces from 3D intraoral scanners,” *IEEE Trans. Med. Imaging*, vol. 39, no. 7, pp. 2440–2450, 2020.
- [7] H. Ben Yedder, T. Attig, and F. Daoudi, “3DTeethLand: A benchmark for 3D dental landmark detection and tooth segmentation,” in *Proc. MICCAI Challenge*, 2024.
- [8] Z. Cui, C. Li, and W. Wang, “ToothNet: Automatic tooth instance segmentation and identification from 3D dental model,” in *Proc. CVPR*, pp. 6368–6377, 2019.
- [9] T. H. Wu, C. Lian, S. Lee, M. Kuijkaas, Y. Heading, and D. Fels, “Two-stage mesh deep learning for automated tooth segmentation and landmark detection from 3D intraoral scans,” *IEEE Trans. Med. Imaging*, vol. 41, no. 11, pp. 3158–3172, 2022.
- [10] L. Zhang, Y. Wang, F. Guo, and D. Gao, “TSGCNet: Discriminative geometric feature learning with two-stream graph convolutional network for 3D dental model segmentation,” in *Proc. CVPR*, pp. 6382–6391, 2021.
- [11] G. Rossini, S. Parrini, T. Castroflorio, A. Deregibus, and C. L. Delatorre, “Efficacy of clear aligners in controlling orthodontic tooth movement: a systematic review,” *Angle Orthod.*, vol. 85, no. 5, pp. 881–889, 2015.
- [12] L. Lombardo, A. Arreghini, F. Ramina, F. Huanca Ghislanzoni, and G. Siciliani, “Predictability of orthodontic movement with Invisalign: a retrospective study,” *Prog. Orthod.*, vol. 18, no. 35, 2017.
- [13] J.-P. Houle, L. Piedade, R. Todescan Jr, and G. Pinheiro, “The predictability of transverse changes with Invisalign,” *Angle Orthod.*, vol. 87, no. 1, pp. 19–24, 2017.
- [14] R. T. Sutton, D. Pincock, D. C. Baumgart, D. C. Sadowski, R. N. Fedorak, and K. I. Kroeker, “An overview of clinical decision support systems: benefits, risks, and strategies for success,” *NPJ Digit. Med.*, vol. 3, no. 17, 2020.

- [15] J. H. Park, T. Hwang, Y. C. Lee, S. H. Dong, and S.-H. Kang, “Automated identification of cephalometric landmarks: Part 1 — Comparisons between the latest deep-learning methods,” *Angle Orthod.*, vol. 89, no. 6, pp. 903–909, 2019.
- [16] X. Wang, J. Mao, and Y. Li, “Deep learning-based prediction of treatment outcomes in orthodontics: A systematic review,” *J. Dent. Res.*, vol. 100, no. 11, pp. 1162–1171, 2021.
- [17] I. Loshchilov and F. Hutter, “Decoupled weight decay regularization,” in *Proc. ICLR*, 2019.
- [18] Y. Zhao, H. Li, S. Wan, A. Sekuboyina, X. Hu, and G. Tringale, “Automatic dental shape analysis and feature extraction,” in *IEEE Int. Conf. Shape Modeling*, pp. 186–195, 2006.
- [19] Y. Kumar, R. Janardan, and B. Larson, “Automatic feature identification in dental meshes,” *Comput.-Aided Des.*, vol. 44, no. 1, pp. 1–12, 2012.